

MOTORVEHICLE UNIVERSITY OF EMILIA ROMAGNA

DIPARTIMENTO DI INGEGNERIA "ENZO FERRARI"

Master's Degree in

ELECTRONIC ENGINEERING FOR INTELLIGENT VEHICLES

Electronic System Design Project

Automotive data logger board with
Li-Ion battery backup supply source

Anno Accademico 2023/2024

Contents

1 Project description	1
1.1 Block scheme layout	2
2 Power section	3
2.1 External power supply plug	3
2.2 Former DC/DC switching converter	4
2.3 Battery Charger	6
2.4 External battery plug	7
2.5 Battery over-discharging protection	8
2.6 Commutator	9
2.7 Latter DC/DC switching converter	10
2.8 Analogue supply voltage source	12
3 Data acquisition section	13
3.1 PT1000	13
3.2 Analogue and digital input	15
4 PCB section	16
4.1 PCB stack-up	16
4.2 PCB layout	17
4.3 MOLEX connectors	18
5 Micro-controller unit section	18
5.1 ADC configuration and normal operation	18
5.2 Logs and saving procedure section	19
6 Final production board	20

1 Project description

The project in collaboration with Ferrari details the procedures, technical aspects, and testing conducted to develop, build, solder a circuit and design its associated printed circuit board. While we made the decision on the micro-controller and integrated circuits, certain requirements and constraints align with Ferrari's guidelines.

The project involves designing a logic board housing a micro-controller that maintains functionality within the temperature range of $0^{\circ}C - 85^{\circ}C$. The logic board is powered externally, with a voltage range of $9V - 16V$ and a nominal value of $14V$. The power section of the logic board must reliably perform the following operations:

- Charge a Li-Ion battery when the external power supply is available.
- Automatically switch from the external power supply to the Li-Ion battery in case of external power failure, and vice versa.
- Transition into a low-power mode after a specified duration.

The logic board must have the capability to store essential logs, such as switching operations performed by the integrated circuit, such as when we start to use the battery, in a non-volatile memory. The logs facilitates system debugging in case of failures, for this reason there are no specifications about which type of logs we need to use. Additionally, the system comprises a data acquisition section and a communication line, following these guidelines:

- The single-ended analog input samples an analog voltage within the range of $0V - 5V$ at a sampling rate of $1kHz$. The read analog voltage must be transmitted through the CAN bus.
- The active-low level digital input samples an analog voltage within the $0V - 5V$ range and translates it into a high-low value at a sampling rate of $10Hz$.
- The PT1000 single-ended sensor reads temperatures within the range of $0^{\circ}C - 150^{\circ}C$. The sampling rate can be determined by us.

The logic board doesn't necessarily need to store all readings in non-volatile memory but must have the capability to transmit them through the CAN bus communication line. The CAN bus bit speed should operate at its maximum capacity: $1Mbps$.

Wherever is possible, it is required to use automotive components, but also protections, safety devices and a robust design procedures.

1.1 Block scheme layout

The block diagram describes the main functionality of the logic board, the flow of energy (grey arrows) and the connection among the different physical plug (blue arrows).

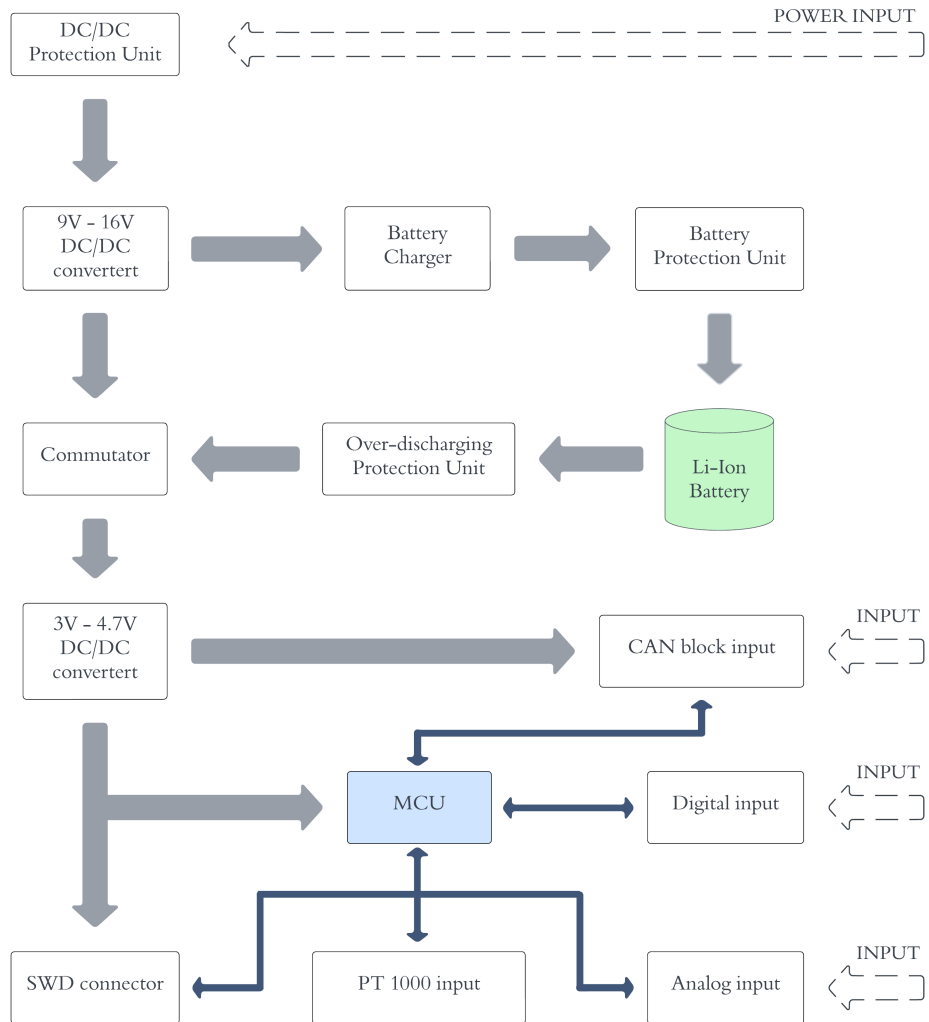


Figure 1: Block diagram

2 Power section

We designed the power section following the specified requirements of the project. We decided to use two different DC/DC switching converter, in order to achieve a high efficiency and to keep a reasonable voltage value inside the circuit to prevent hazardous situation.

Furthermore in the power chapter, two different tools have been used to test and simulate the behaviour of the selected circuit parts to increase the reliability of the project:

- WEBENCH® Circuit Designer: is a Texas Instrument tools that creates the environment with end-to-end selection, design, and simulation capabilities.
- LTspice®: is a powerful and fast SPICE simulator software, schematic capture and waveform viewer.

Every components in the schematic is automotive-grade compliant, unless otherwise specified.

The next chapter will provide a brief description of the main blocks of the circuit schematic, highlighting the most crucial technical choices made.

2.1 External power supply plug

The initial block holds paramount importance in the power section domain, particularly concerning safety issues and electrical protection.

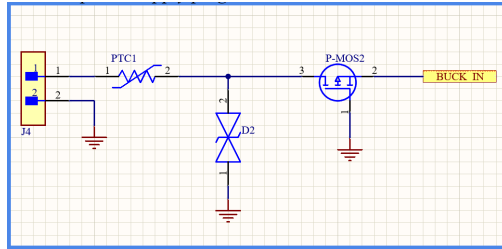


Figure 2: Protection circuit for external power supply plug

Various components have been strategically employed to prevent three potentially unsafe situations:

- Over-current protection: a positive temperature coefficient thermistor start to act as an open circuit when the current exceed $750mA$ for more than 20 seconds or immediately if the current surpasses the trip value, set at $1.5A$.
- Bidirectional voltage suppressor diode: it is designed to safeguard voltage-sensitive components from high-voltage, high-energy transients.
- P-MOSFET: in this configuration, the P-MOS with the gate pin clamped to ground prevents reverse polarity power connections, up to $30V$.

The output port of this section is connected to the input port of the first DC/DC converter.

2.2 Former DC/DC switching converter

The first DC/DC has been chosen to satisfy the requirements of the project, specifically to work in the working voltage window of [9V – 16V]. The schematic of the switching converter is depicted in the following image:

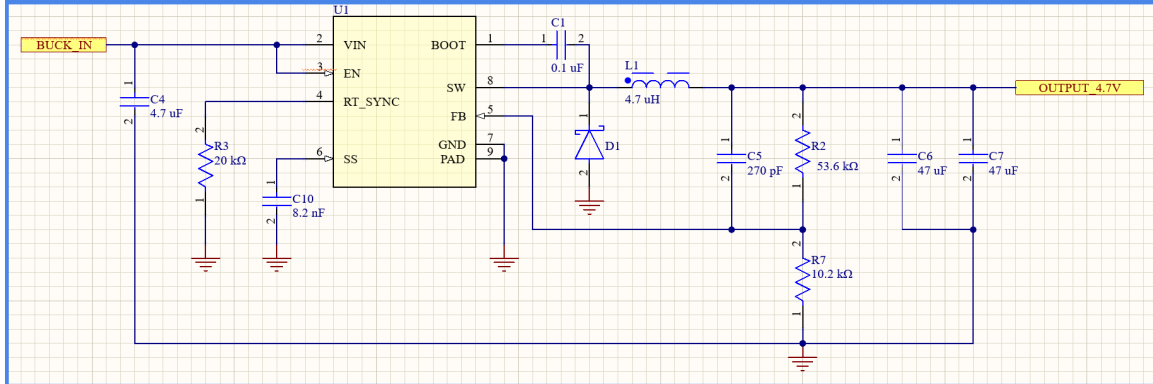


Figure 3: 4.7V DC/DC switching converter

The integrated circuit *LMR14020 – Q1*, referred to as *U1* in the schematic, is an automotive-grade step-down converter. In our application, it is configured to reduce the input voltage to a 4.7V output. The design of the external power supply plug ensures that it does not exceed the maximum ratings of the switching IC, preventing potential permanent damage to the device. The relevant absolute Maximum Ratings include:

- Input Voltages (V_{IN} , EN to GND): MIN $-0.3V$ MAX $44V$
- Input Voltages ($BOOT$ to GND): MIN $-0.3V$ MAX $49V$

Our protection measures not only limit the input to the specified maximum ratings but also maintain the V_{IN} voltage within the Recommended Operating Conditions, ranging from 4V to 40V. This compliance fully satisfies the voltage window requirement.

A set of simulation has been made using the WEBENCH® Circuit Designer tool:

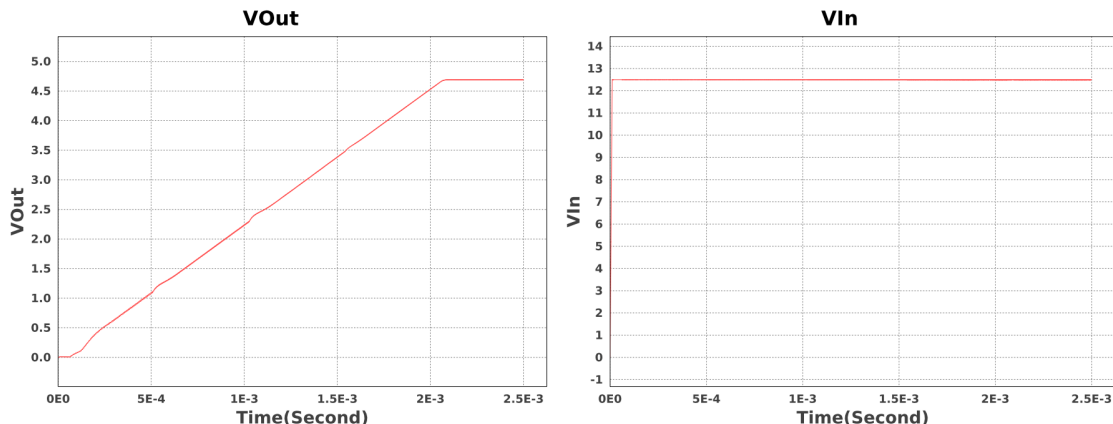


Figure 4: 1st DC/DC Startup

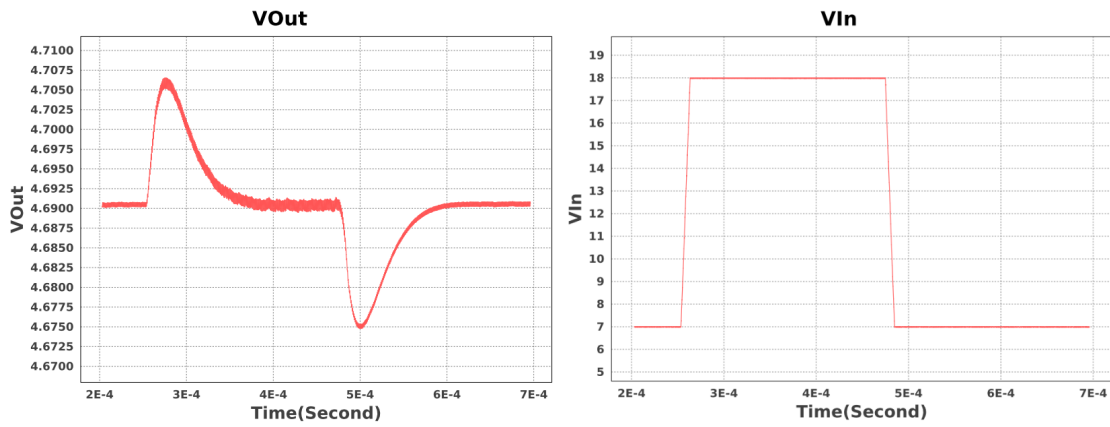


Figure 5: 1st DC/DC input transient

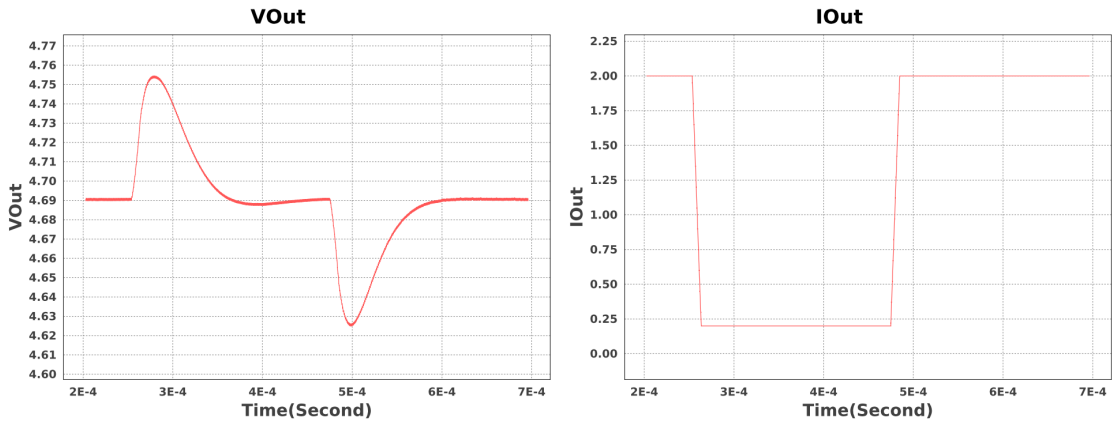


Figure 6: 1st DC/DC load transient

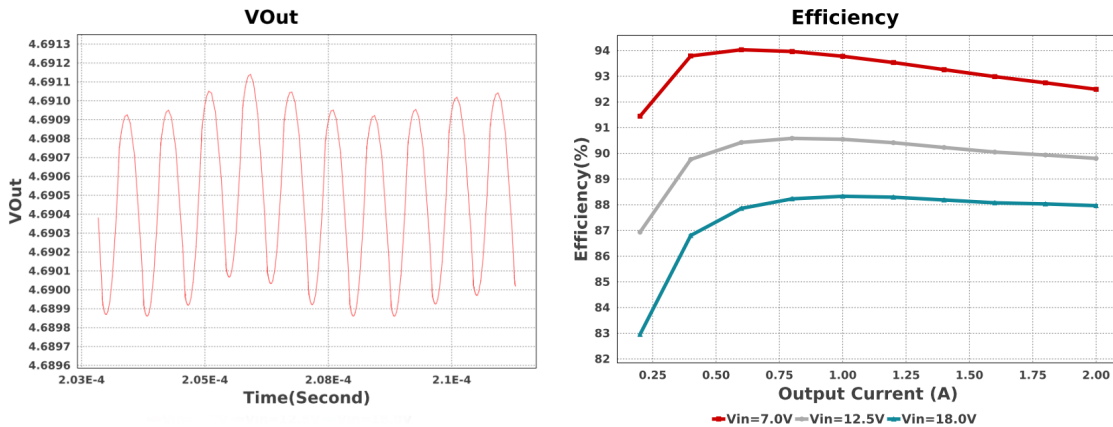


Figure 7: 1st DC/DC Steady state and efficiency

Further details about the simulation are stored in the documents generated by the Texas Instruments ModelSim software.

ments tool. In summary, the final results are as follows:

- 88% of efficiency.
- 1.18mV peak to peak output voltage.
- 2A maximum output current.
- 1.81ms startup time.

A detailed analysis of the current consumption will be conducted later to showcase the IC's ability to power up the entire circuit.

2.3 Battery Charger

The IC battery charger *BQ25171 – Q1* is responsible for receiving power from the first DC/DC switching converter and controlling the state of charge of the cell. In our project, we chose to use a 18650 format 3.7V lithium battery cell. Since no specific rules are set, we opted for this common format size to facilitate cell swapping and accommodate the use of multiple brands.

The state of charge of the cell mentioned earlier is the level of charge of an electric battery relative to its capacity and expressed in voltage.

The automotive-grade battery charger allows to use three different chemistry (*Li+*, *NiMH* and *LiFePO₄*), sets various charge timers (to prevent hazardous situation) and offers different charge voltage settings. Thanks to this, we can charge up to two *Li+* cells and up to six *LiFePO₄*.

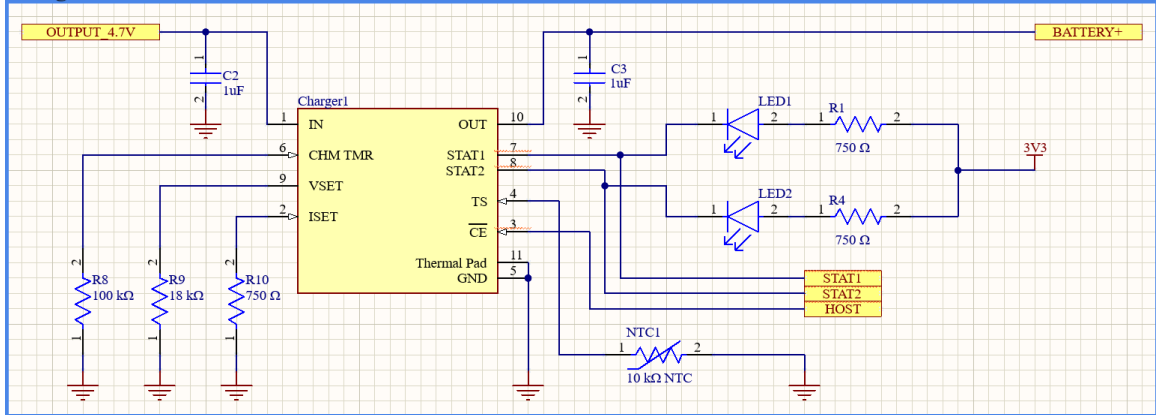


Figure 8: Battery charger

As mentioned earlier, the input voltage of the battery charger is 4.7V, falling within the recommended operating condition [3V – 18V] of the manufacturer. The IC charges the battery using a linear voltage regulator. Furthermore, we can calculate the minimum and the maximum efficiency of the IC, respectively 64% when the battery reaches 3V and 89% when the battery reaches 4.2V.

It's crucial to highlight the decision to choose 4.7V as the output of the first DC/DC switching converter. The decision is guided by the aim to minimise power dissipation and maximise efficiency. The voltage (4.7V) at the input of the IC considers the voltage dropout current at the maximum ambient operating temperature range [0° – 85°], as shown below:

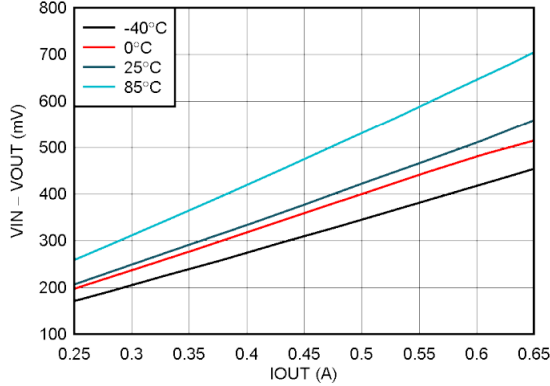


Figure 9: Dropout voltage vs output current

The worst-case scenario reveals a dropout voltage of approximately $420mV$ at 85° , resulting in a maximum output voltage of $4.28V$, which is sufficient to charge the lithium cell.

The circuit has the following protection features:

- Safety timer: set at 10 hours. If exceeded, the charging process is automatically halted. The timer can be reset using the HOST pin connected to the micro-controller or it is automatically reset every time the external power supply is disconnected.
- Negative temperature coefficient thermistor: it senses the temperature of the cell and stops the charge if it exceeds the $[0^\circ C - 45^\circ C]$ window.
- Output over-current protection: a resistor sets the maximum current charging rate at $400mA$.
- Input and output over-voltage protection.

The IC enables tracking of all possible fault conditions, activating the two LED's on the PCB board. Additionally, we collect this information through the micro-controller and save it in the memory as data log.

2.4 External battery plug

Starting from this block, the primary goal of the project is to minimise power consumption as much as possible. Careful attention is given to controlling every loss to increase efficiency, ensuring a longer circuit lifetime when the external power supply is not available.

The protection on the external battery follows the same principle as the protection applied to the external power supply. We decided to remove the PTC thermistor since it dissipates power, and the next block, the commutator, already includes an over-current protection system.

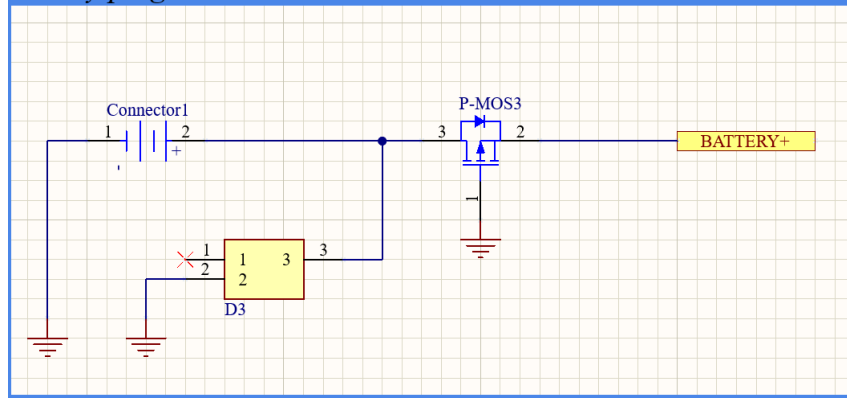


Figure 10: External battery plug

Reverse polarity protection is still required because the battery charger lacks protection on the output pin. By using the P-MOSFET, we prevent the supply of a negative voltage, maintaining a consumption of $9\mu W$ with a flowing current of $10mA$.

2.5 Battery over-discharging protection

While the battery charger provides over-voltage and over-current protection, there is no supervision on the minimum voltage of the external battery. Since it is not possible to physically disconnect the battery, we integrate a IC supervisor *BD5330G – 2MTR* into our circuit. The IC checks the state of charge of the battery (in V) and controls the threshold beyond which we must not go.

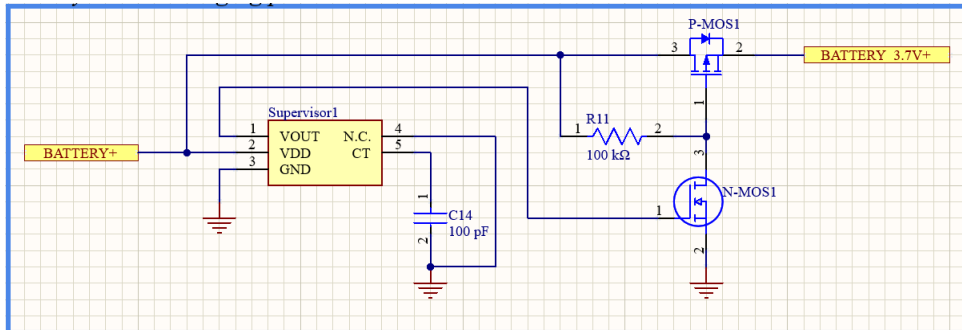


Figure 11: Supervisor circuit

The supervisor circuit has a C-MOS configuration, providing the voltage of the battery to the N-MOS (and thus activating the P-MOS) when we are above the threshold of $3V$. Otherwise, it connects to the ground and safeguards the state of charge of the battery.

Different configurations exist for the voltage threshold. In our project we decided to preserve the cell for long-time disconnection: with $100mAh$ remaining and a consumption of $1\mu A$ in the worst condition, we guarantee a battery lifetime of more than 10 years.

To prevent disconnection with the charger and maintain the possibility to charge the battery in any case, over-discharging protection is placed between the cell and the commutator.

2.6 Commutator

The commutator has the critical role of sensing the external power supply voltage and the external battery plug, then selecting the output among the two possibilities.

The reason why we decided to implement the first DC/DC converter now becomes clearer: to avoid high variations in voltage, we use a lower and safer internal voltage value that can be interchanged with the battery voltage. In the worst-case scenario, we might experience the disconnection of the external power supply at 16V and the external battery at 3.1V nominal. In this case-study, the actual voltage drop will be 1.6V at the input of the second DC/DC converter (because the first DC/DC converter step down the voltage at 4.7V), which is completely acceptable and compliant with the recommended ratings condition, as we will discuss later.

The IC commutator *TPS2115A – Q1* is an automotive-grade auto-switching power multiplexer. It provides two protection features for the circuit:

- Reverse and Cross-Conduction Blocking: to prevent current flowing back into the lower voltage supply, the device does not connect it to the output until the output voltage has fallen to within 100mV of the supply voltage.
- Adjustable Current Limit: set by a resistor to limit the maximum current up to 0.67A.

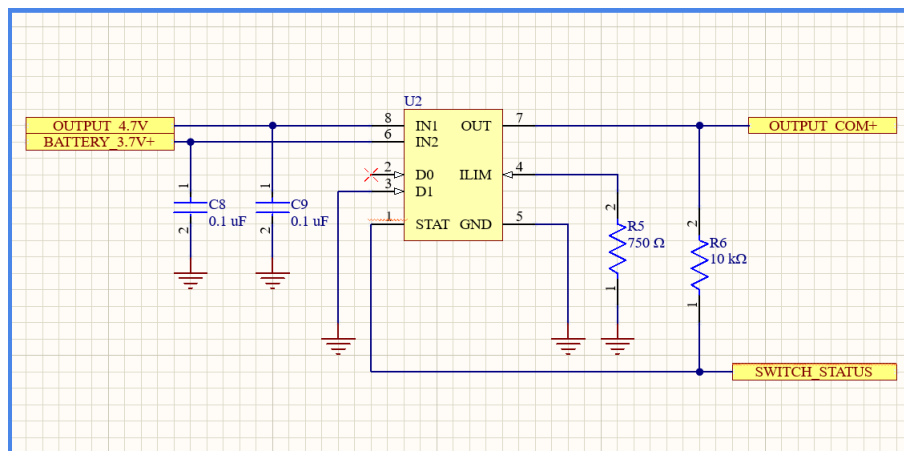


Figure 12: Commutator circuit

The typical operating current of the circuit is $55\mu A$ while the drain-source resistance of the internal MOSFET is $84m\Omega$: the total consumption with a $10mA$ flowing current is around $0.2mW$. The efficiency improvement compared to a Schottky diode, which operates at a voltage of $0.4V$ is 20 times greater.

The SWITCH_STATUS port is connected to the micro-controller in order to verify and save which power supply have is connected to the output of the commutator.

2.7 Latter DC/DC switching converter

The final block in the power section is the second DC/DC converter, designed to receive input voltage from the commutator and deliver a stable output voltage. This stable output voltage is crucial as it will power the micro-controller, the CAN bus block, and the OPAMP of the PT1000 reading block.

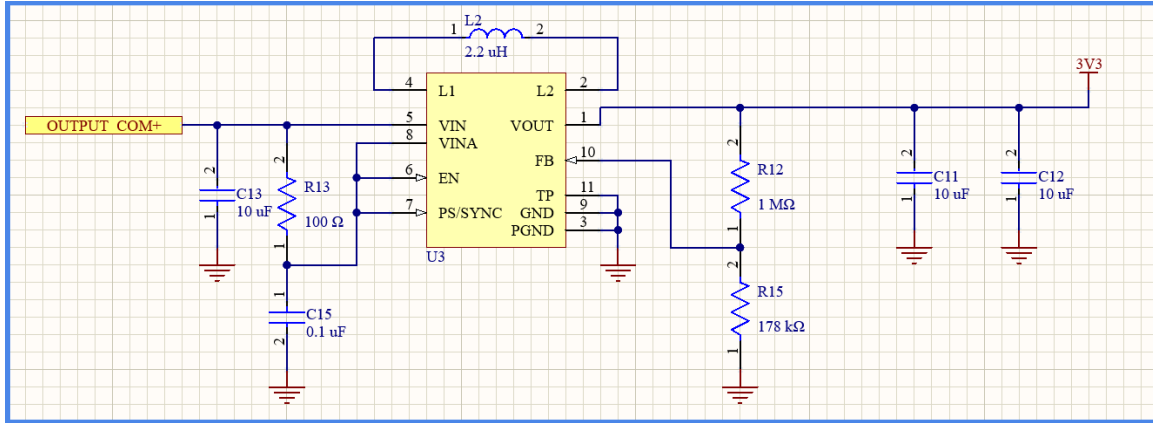


Figure 13: 3.3V DC/DC switching converter

The input voltage accommodates a variable range, spanning from 3V (the lowest operating voltage of the battery) to 4.7V (when the entire circuit is powered by an external power supply).

Additionally, it is required that the switching converter's efficiency and energy consumption are optimised to achieve the lowest overall power consumption.

The following images show the results of the switching converter, taking into account the variable input voltage mentioned earlier. The simulations were conducted with a reference output current of 300mA, although it's important to note that the switching converter can handle a maximum output current of up to 800mA:

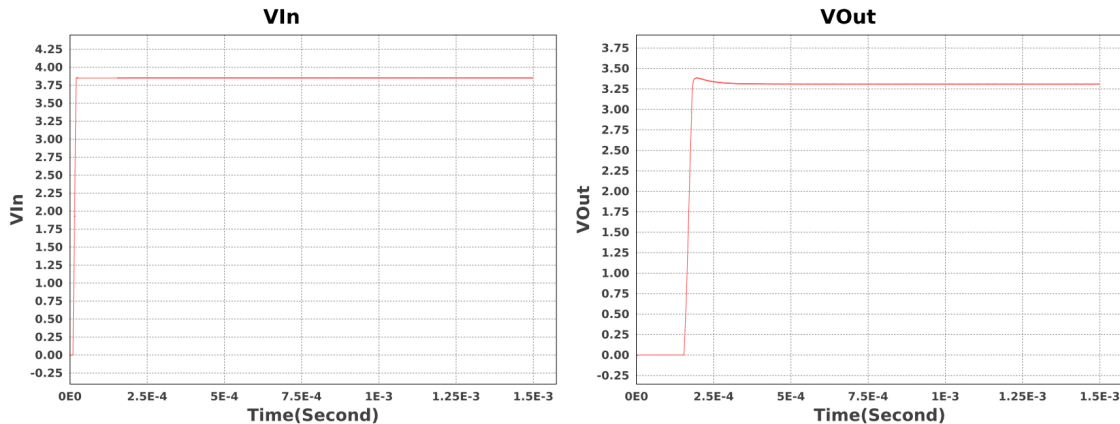


Figure 14: 2nd DC/DC convert startup

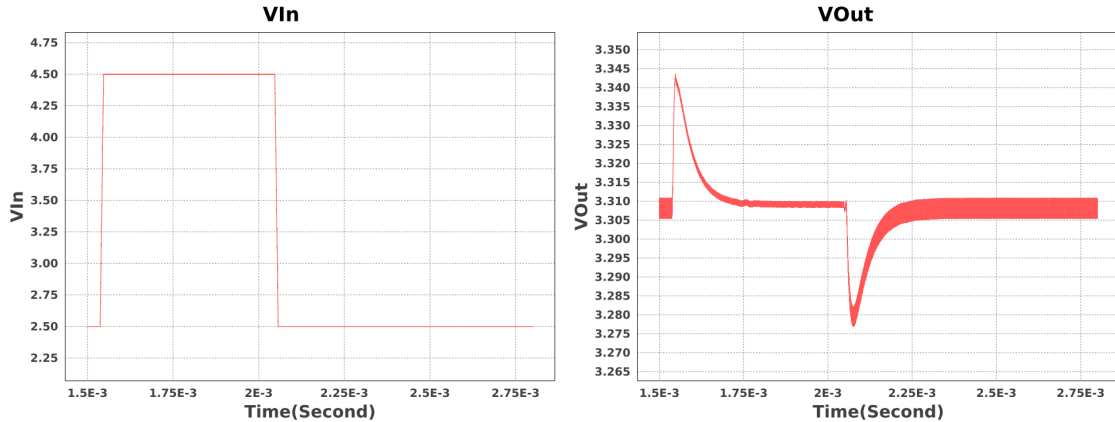


Figure 15: 2nd DC/DC input transient

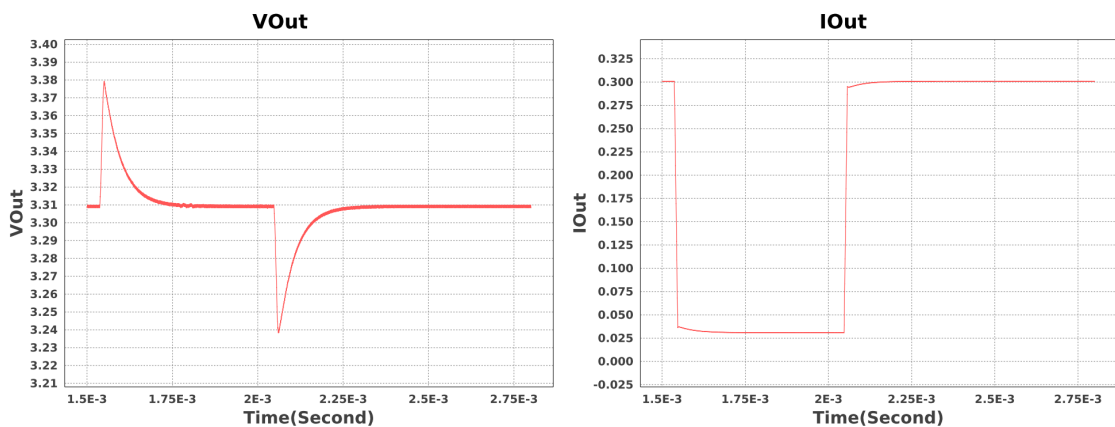


Figure 16: 2nd DC/DC load transient

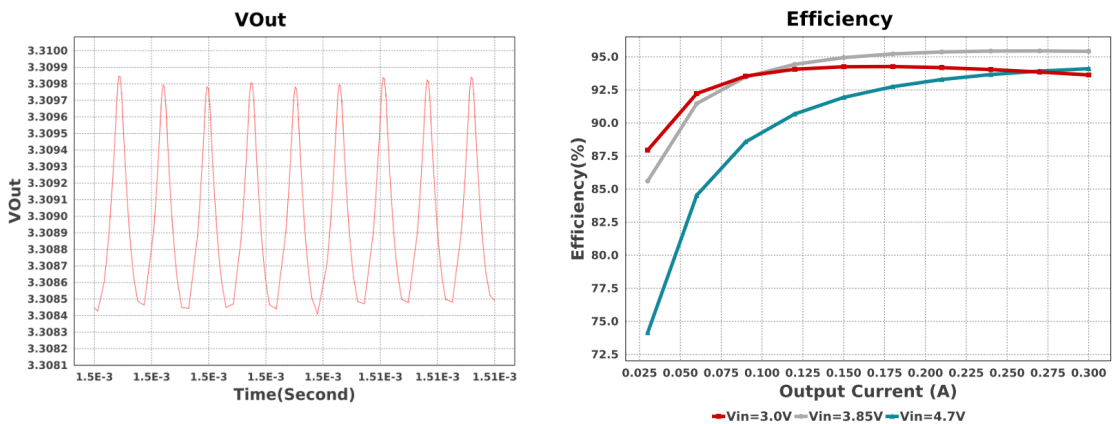


Figure 17: 2nd DC/DC steady state and efficiency

Further details about the simulation are stored in the documents generated by the Texas Instruments tool. In summary, the final results are as follows:

- 93.7% of efficiency.
- $1.28mV$ peak to peak output voltage.
- 0.8A maximum output current.
- $1.35MHz$ switching frequency.

The switching frequency is crucial as it allows for the development of a low-pass LC filter before the input of the analog voltage into the micro-controller.

2.8 Analogue supply voltage source

The micro-controller has various voltage supply pins to power up the different sections. Moreover, an analog supply pin is reserved to the analog section and serves as a reference for various operations, such as the analog-to-digital converter. Increased fluctuations in the analog voltage pin not only reduce the accuracy of readings from these modules but can also lead to malfunction in the micro-controller.

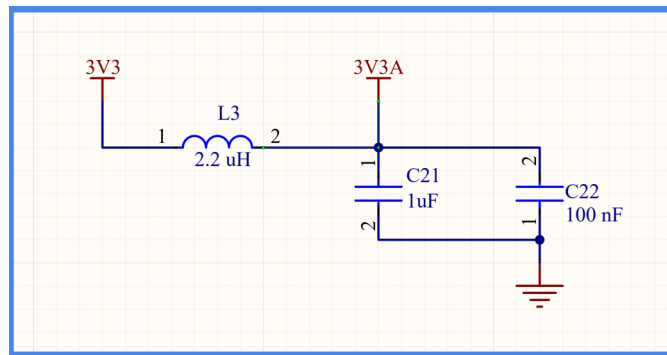


Figure 18: LC filter for analogue supply voltage

The more convenient way to reduce the ripple generated by the latter DC/DC converter is by integrating a low-pass filter.

As we discover from the simulation, the ripple generated has a $1.3mV$ voltage amplitude at $1.35MHz$ frequency. We opted to implement a second-order LC filter as our choice for the low-pass filter. After replicating the ripple and output voltage frequency of the DC/DC switching converter using LTspice[®], the results demonstrate a notable improvement in the final ripple:

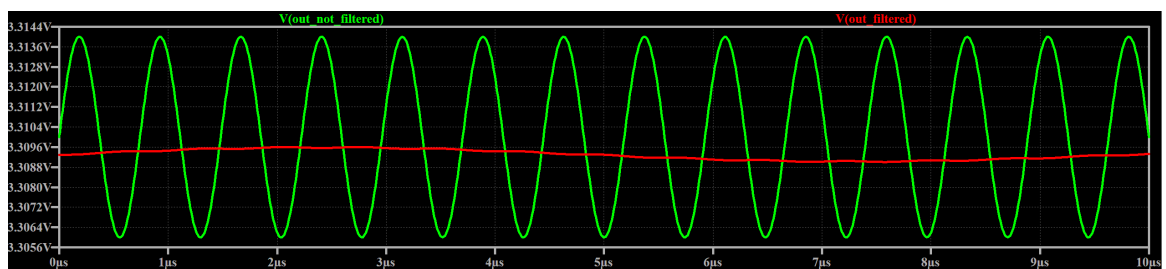


Figure 19: LC filter for Analogue voltage supply

We carefully chosen a low-impedance inductance ($64m\Omega$) to minimise the losses in the LC filter and maintain proximity to the reference voltage.

3 Data acquisition section

3.1 PT1000

In order to acquire the temperature measurement provided by the PT1000 sensor, the three wire scheme in Figure 3.1 has been adopted. The circuit uses a low offset operational amplifier in a non-inverting configuration with inverting reference, in order to offset and amplify the signal, which helps to use the full ADC resolution and increase measurement accuracy.

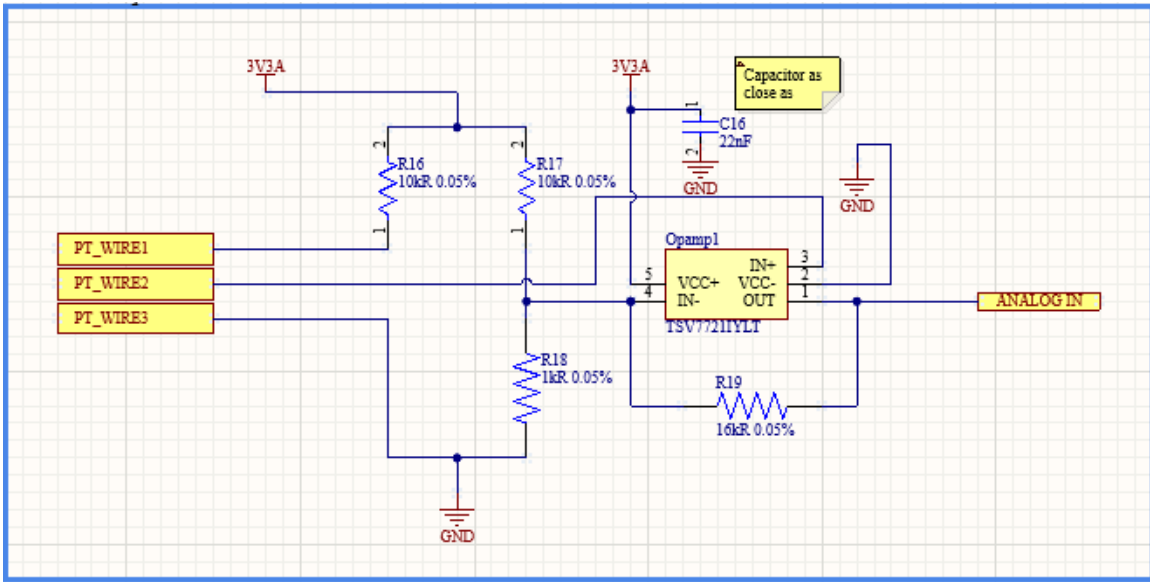


Figure 20: PT1000 acquisition circuit.

The resistors have been chosen with very fine tolerances, compatibly with the budget, in order to reduce as much as possible the measurement uncertainty associated to the temperature reading. The analytical evaluation of the latter has shown that the resolution of the 13 bit ADC of the STM32L433CCT3 is more than enough, considering the 3.3V single power supply. As mentioned before, in order to increase as much as possible the dynamic range of the ADC input, we selected a rail-to-rail operational amplifier, with a linear output swing between 0.025V and 3.275V.

Considering that the client specified the operating range of the sensor between 0 and 150°C , we tuned the differential amplifier gain to maximize the temperature sensitivity, maintaining some positive and negative margins for possible out-of-range values.

The performances of the circuit have been evaluated by means of Spice simulations. More specifically, Two types of simulations were conducted, the first related to the amplifier's output range, and the second concerning the impact of resistor tolerances. In Figure 21, the operational amplifier's output swing is shown as a function of the PT1000 resistance. In Figure 3.1, we can observe, for a fixed sensor resistance value, the output voltages obtained for all the extreme combinations of resistor

tolerances. This latter simulation highlights the worst-case scenario of the error due to tolerances, which will be subsequently eliminated through software calibration.



Figure 21: PT1000 acquisition circuit: output range

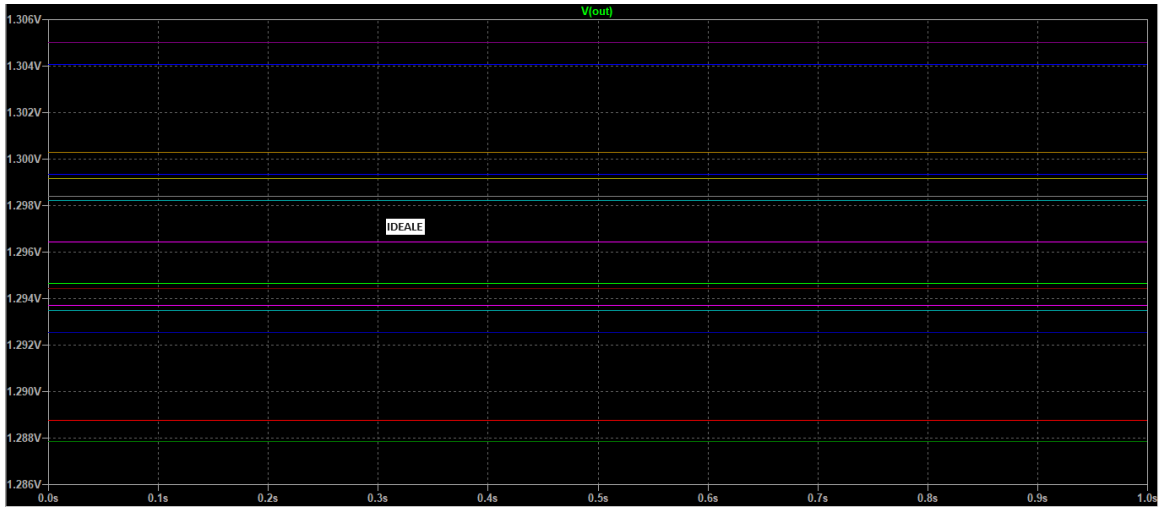


Figure 22: PT1000 acquisition circuit: tolerance-related error simulation.

The formula for the amplifier gain is the following:

$$G_{amp} = \frac{(R_{17}/R_{18}) \times R_{19}}{(R_{17}/R_{18})}. \quad (1)$$

Consequently, the transfer function of the non inverting amplifier is

$$V_{OUT} = V_{CC} \times \frac{R_{PT1000}}{R_{PT1000} + R_{16}} \times G_{amp} - \left(\frac{R_{19}}{R_{17}} \times V_{CC} \right). \quad (2)$$

Therefore, the achieved sensitivity in the measurement range is

$$S = \frac{V_{OUT}(150^{\circ}C) - V_{OUT}(150^{\circ}C)}{150^{\circ}C} = \frac{3.15V}{150^{\circ}C} = 19mV/^{\circ}C \quad (3)$$

The choice of the amplifier deserves special mention. For this type of application, instrumentation differential amplifiers are widely adopted in the literature, offering generally superior metrological performance, including high input resistance at the two terminals. In this regard, the use of the INA321 integrated circuit was evaluated through simulations. The INA321 would allow for an approximately 10% increase in circuit sensitivity; however, the measurement uncertainty would increase due to the greater number of resistors needed to achieve the required gain. Furthermore, the offset voltage declared by the manufacturer is higher than that of the TSV7721 by at least one order of magnitude (500 μ V compared to 50 μ V). This could introduce a significant error, impossible to compensate for without further complicating the circuit (resulting in higher costs). Finally, although the INA321 is relatively low-cost, the solution based on the TSV7721 allows for a cost reduction of at least three times. One last consideration is dedicated to the use of a three wire PT1000. This particular configuration allows us to compensate for the sensor's wires resistance, which determines a non negligible error in typical two wires schemes. This choice has been made to increase accuracy, even though PT1000 is inherently more robust to wiring resistance with respect to other versions, like PT100, as a consequence of the higher nominal resistance value.

3.2 Analogue and digital input

The circuit needs to accept two different types of input: one analogue and one digital input, with two distinct sampling frequencies: 1kHz for the analogue input and 10Hz for the digital input.

Considering the micro-controller's internal 12-bit analog-to-digital converter, we opted to sample the analogue voltage value using a voltage divider, scaling down the maximum voltage to 3.28V, to comply with the micro-controller's constraints. This approximation allows for a minimum readable difference of 0.8mV within the 3.3V. Therefore the real minimum input voltage variation readable is 1.33mV in the 5V scale.

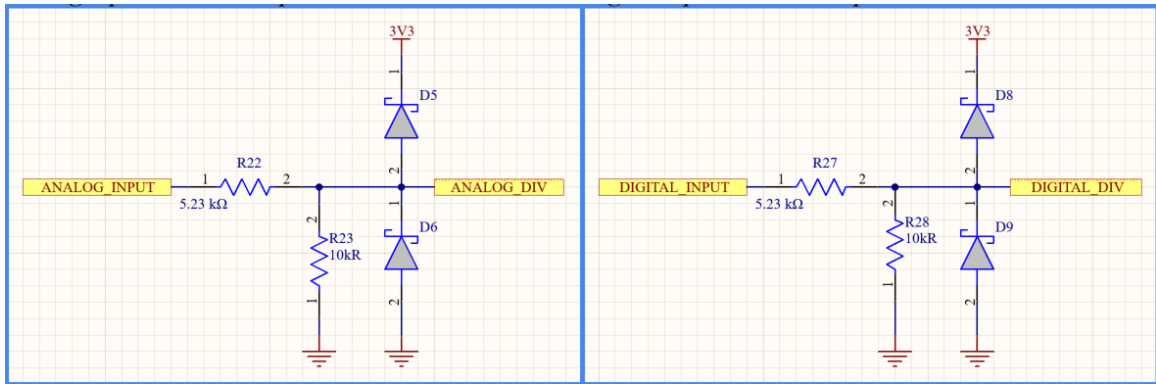


Figure 23: Analogue and digital input circuit.

Since we are directly exposing two micro-controller connections to the external environment, a simple protection circuit is necessary to prevent supplying the micro-controller with a voltage rate

that exceeds the absolute maximum ratings, potentially causing permanent damage.

The protection circuit comprises two Schottky diodes connected to the supply voltage provided by the DC/DC converter and the ground. This configuration ensures that the voltage supplied remains within the [0V – 3.3V] range, preventing any possibility of exceeding this range.



Figure 24: Analogue and digital simulation

The simulation demonstrate the conversion from the 5V to the 3.3V and the protection to over-voltage and under-voltage input.

4 PCB section

In this section, we aim to briefly discuss the key decisions made to achieve a well-structured PCB layout, optimising space and minimising EMI interference generated by noisy components, and ensure the safety of the circuit board.

As no specific guidelines were requested, we pursued various strategic paths to ensure a balanced trade-off between the cost and performance of the printed circuit board.

4.1 PCB stack-up

The PCB has a 4-layer stack-up: signal - ground - ground - signal. This specific combination provides a high EMI attenuation among the 2 signal layers and gives to this 2 layers a close reference to the ground.

	Top Overlay	Overlay	
1	Top Solder	Solder Mask	0.0254mm
2	Top Surface Finish	Surface Finish	0.02mm
3	Top Layer	Signal	0.035mm
4	Dielectric 1	Prepreg	0.2104mm
5	Int1 (GND)	Signal	0.0152mm
6	Dielectric 3	Core	1.065mm
7	Int2 (GND)	Signal	0.0152mm
8	Dielectric 5	Prepreg	0.2104mm
9	Bottom Layer	Signal	0.035mm
10	Bottom Surface...	Surface Finish	0.02mm
11	Bottom Solder	Solder Mask	0.0254mm
12	Bottom Overlay	Overlay	

Figure 25: PCB stack-up layout

The thickness of the different layers follows the capabilities of the manufacturer.

A congruent number of via stitching has been added to the PCB. As our project does not involve high-frequency signals, there are no specific rules regarding the spacing and size of the vias. The main purpose of the via stitching is to establish a solid connection between the two ground layers, ensuring a consistent reference throughout.

4.2 PCB layout

The PCB layout has been structured to properly separate the power section from the signal section. This arrangement aims to minimise and bound the EMI interference originating from the two DC/DC switching converters.

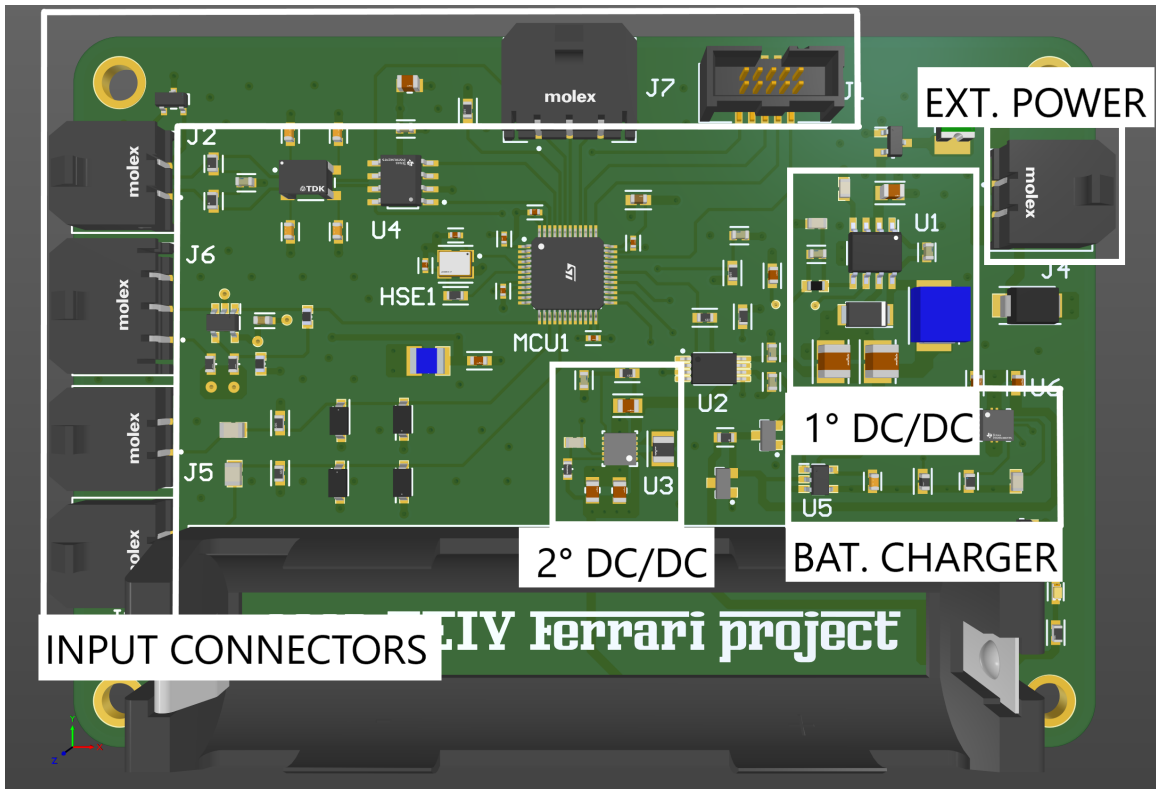


Figure 26: PCB section division

The commutator switch is located between the two DC/DC converters to facilitate the transition in case the external power supply stops to source the circuit. Furthermore, the CAN bus is strategically placed away from the DC/DC converters and other sources of potential electromagnetic interference.

The two connectors situated on the top of the board serve the purpose of flashing the board and enabling real-time visualisation of various inputs.

The entire circuit has been meticulously routed on a printed circuit board measuring 10cm by 7cm printed circuit board, significantly reducing production costs by a factor of 4 (since the PCB price tends to rise quickly beyond the 10cm x 10cm dimension).

4.3 MOLEX connectors

Redundancy in safety measures is imperative. In our PCB design, we employ MOLEX connectors for all plugs, with the exception of the battery slot and the SWD connector utilized for MCU flashing.



Figure 27: Female and male 2 positions MOLEX connector

While our system includes safeguards against polarity inversion, these connectors prevent incorrect plug insertion by design. Additionally, the physical structure prevents the insertion of a 2-position connector into a 3-position connector due to their slightly different shapes, ensuring a foolproof connection.

5 Micro-controller unit section

The micro-controller has been chosen to properly satisfy the functionality of the entire logic board. The *STM32L433CCT3* guarantee the optimal trade-off between performance and energy consumption. Moreover, it has the following features:

- Ultra-low-power with FlexPowerControl.
- Up to 256 KB single bank Flash, also used to store some data log.
- 12-bit ADC, up to 16-bit with hardware oversampling.
- $[-40^{\circ}\text{C}, +125^{\circ}\text{C}]$ temperature range.
- CAN interface up to 1Mbps.

The programming of the micro-controller is essential to ensure stable operation and excellent performance in terms of power consumption, as well as reliability in data reading. We'll be discussing some of the most crucial components that we've analysed during the coding process.

5.1 ADC configuration and normal operation

One of the main functionalities of the board is to manage the acquisition of the analog input and the Pt1000 input. This task is in charge of the 12 bit ADC integrated into the microcontroller. To fulfil the specification's constraint on the sampling frequency of the analog input, that is fixed at 1 KHz, the ADC has been configured to be triggered by a timer that expires every 1 ms and, consequently,

generates an interrupt. This interrupt activate the ADC sampling and conversion of the analog input channel first and then of the Pt1000 channel. The choice of sampling the Pt1000 data at 1 KHz is bounded to the fact that the *STM32L433CCT3* microcontroller is provided with a single ADC. Since this sampling frequency is way beyond the rate at which the temperature measured by the Pt1000 can change, it has been decided to compute a representative mean value of the temperature after collecting 10000 samples. The raw values provided at the ADC output are then converted into a voltage for the analog input and into a temperature for the Pt1000.

$$T = \frac{R_{Pt1000} - R_0}{\beta} \quad (4)$$

$$\beta = 3.85 \frac{\Omega}{^{\circ}C} \quad (5)$$

In the end both these values are transmitted by means of the CAN bus.

5.2 Logs and saving procedure section

During debugging, certain logs are essential for obtaining a clear overview of the historical behaviour of the micro-controller. Our circuit incorporates three inputs from the charger and the commutator: we can detect when the external power is switched off and the battery is used as the source for the entire circuit. Furthermore, two signals distinguish among four different scenarios in which the charger might operate.

CHARGING STATE
Charge completed, charger in sleep mode or charge disabled (including $V_{OUT} > V_{RECHG}$ after TMR_EXP for NiMH charging)
Normal charge in progress (including intermittent charge active for NiMH, and automatic recharge for Li+ charger)
Recoverable fault (VIN OVP, BAT OVP, TS HOT, TS COLD, TSHUT)
Non-recoverable or latch-off fault (VSET/CHM_TMR/ISET pin short/open, BAT OCP, TMR_EXP for Li+ charging, $V_{OUT} < V_{RECHG}$ after TMR_EXP for NiMH charging)

Figure 28: Charging Status Indicator

Interrupts are configured to detect every state switch of these inputs, then stored in the memory with an attached timestamp. The timestamp is retrieved by exploiting the integrated RTC inside the microcontroller. The *STM32L433* micro-controller we've implemented does not include a dedicated EEPROM memory. This decision was made for at least four reasons: to lower the board's cost, minimise PCB space usage, reduce potential faults from additional required components, and, most importantly, due to the absence of a specific need for external memory. The essential log data can be easily stored in no more than 8 bytes, inclusive of the timestamp. [see figure for a typical log line]

A few words should be dedicated to demonstrate the possibility of using the FLASH memory while maintaining the MCU's strong reliability. In theory, using the FLASH memory to save data is not

recommended because it has a limited number of writing cycles, in our case at least 10k cycles. To optimise the save of the data in the FLASH memory, we implement a EEPROM emulation library from ST-Microelectronics and tailor-made for our project, which integrates two autonomous algorithm to distribute the write and the erase in the whole memory.

If we reserve 32 Kbytes of memory for the code, we're left with 112 pages, each having a capacity of 2048 bytes. Assuming an average of 100 logs per day:

1. Each log occupies 4 bytes for data and charger state, which becomes 8 bytes considering the CRC and virtual address. In total, we write 800 bytes per day, rounded up to 1024 bytes. Note that the implementation of CRC offers an extra layer of protection to the log, typically not delivered with the same level of robustness in standard EEPROM.
2. With 112 pages initially available, this effectively becomes 56 pages because a second set of pages, of the same size, is necessary to transfer data when the first set is full.
3. Considering at least 10,000 cycles for each page and performing the erasing operation only when the page is full (every 2 days), we have more than 1000 years before exceeding the Flash memory endurance provided by the manufacturer. This calculation demonstrates that we can safely store a considerable amount of data while maintaining good memory protection.

An interesting point to note is the arrangement of the logs: to avoid cycling through memory excessively, logs are stored consecutively. This approach ensures that until we've written on all 56 pages, we maintain the information from the first page written. Consequently, this enables us to maintain a history of logs for more than 100 days.

6 Final production board

In this section we want to briefly discuss some improvements and change that can be done in the final production board.

- Battery: Our prototype utilised a 18650 battery cell. To adhere to automotive constraints, any 3.7V Lithium battery variant can be employed, ensuring a secure attachment to the PCB and ensuring durability against vibrations..
- Connectors for debugging: SWD and UART connectors were used for debugging and real-time visualisation in our prototype. However, in the production version, these connectors are unnecessary and can be omitted. MCU flashing can be executed before soldering, or using flat pin without having a physical connector:

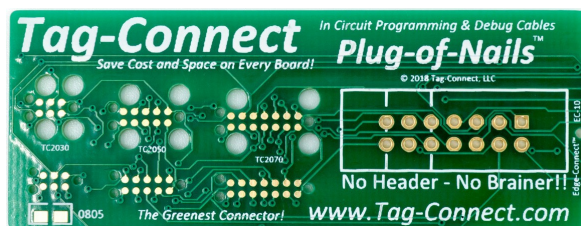


Figure 29: Different TAG connectors pin

- Input and CAN connectors: while the current Molex connectors ensure robust connections between the PCB and cables, because of their closeness, a single connector might be used as a replacement. This improvement could save time, reduce costs, and minimise the board's size.
- Spacing: the spacing between components hasn't been entirely optimised. This decision was taken as a precaution due to the team's inexperienced soldering skills and the limited hardware available for soldering the components together. We are confident that this project will serve as a learning opportunity to enhance our soldering capabilities.